Low-frequency dielectric relaxations of a nonchiral liquid crystal, 8CB

2001 J. Phys.: Condens. Matter 13 4435

(http://iopscience.iop.org/0953-8984/13/20/305)

INSTITUTE OF PHYSICS PUBLISHING JOURNAL OF PHYSICS: CONDENSED MATTER

J. Phys.: Condens. Matter **13** (2001) 4435–4446 www.iop.org/Journals/cm PII: S0953-8984(01)17349-2

Low-frequency dielectric relaxations of a nonchiral liquid crystal, 8CB

Min Young Jin and Jong-Jean Kim[1]

Physics Department, Korea Advanced Institute of Science and Technology, Taejon 305-701, Korea

E-mail: s_phasetr@cais.kaist.ac.kr (Min Young Jin) and jjkim@cais.kaist.ac.kr (Jong-Jean Kim)

Received 19 September 2000, in final form 6 March 2001

Abstract

Low-frequency dielectric measurements are performed on a nonchiral liquid crystal (8CB) for two different cell thicknesses 4.5 μm and 1.6 μm, as functions of temperature at various amplitudes of the probe field. Relaxation peak frequencies are observed at ∼10 Hz for the 4.5 μm thick sample and ∼100 Hz for the 1.6 μm cell. When the external-field amplitude was increased, the relaxation peak frequency was shifted to lower frequency for the 4.5 μm cell but hardly changed for the 1.6 μm cell. To explain this odd result from experimental observations, we performed a numerical simulation, where the ionic impurities were assumed to encounter ionization–recombination processes in addition to a translational diffusion. We were able to confirm that there are two separate contributions from ionic impurities to the low-frequency dielectric relaxations in this system—that is, from fast ions in the single-particle diffusion and slow ions in the ionization–recombination-assisted diffusion.

1. Introduction

A typical dielectric dispersion spectrum of a nonchiral liquid crystal has two distinct parts consisting of a high-frequency part attributed to molecular rotations [1,2] and a low-frequency part with $\varepsilon''(\omega) \propto \sigma/\omega$ due to an ionic impurity contribution [3]. However, very recently a Debye-like relaxation was found in this nonchiral liquid-crystal system at very low frequency beyond the low-frequency conductivity relaxation [4]. This Debye-like low-frequency relaxation was then attributed to a space-charge accumulation in the surface alignment layer, but a porous system was also shown to have a similar low-frequency relaxation due to a pore-to-pore hopping conductivity [5].

The space-charge relaxation process due to ionic impurity diffusion is described by

$$\frac{\partial n}{\partial t} = D\frac{\partial^2 n}{\partial x^2} - \mu\frac{\partial}{\partial x}\left(n\frac{\partial V}{\partial x}\right) \tag{1}$$

[1] Author to whom any correspondence should be addressed.

0953-8984/01/204435+12$30.00

where $n(x,t)$ represents the impurity concentration, D the diffusion constant, μ the mobility, and $V(x,t)$ the electrical potential.

With the condition of zero current density at the surface and an appropriate change of variables into reduced variables of dimensionless units, we can solve the equation and derive the dielectric constant function $\varepsilon^*(\omega)$ of the system as follows [6]:

$$\varepsilon^*(\omega) = \varepsilon_s \frac{\delta^2 + \mathrm{i}\omega}{\mathrm{i}\omega + \delta^2 \tanh(Y)/Y} \tag{2}$$

where ε_s represents the static dielectric constant, $\delta = d/\lambda$ a cell parameter, $\lambda = \sqrt{D\tau_c}$ the diffusion length, $\tau_c = \varepsilon_s/(n_o \mu e)$ the conductivity relaxation time, d the cell thickness, $Y = \sqrt{\delta^2 + \mathrm{i}\omega}/2$, n_0 is the time average of $n(x,t)$, μ is the mobility, e is the ionic charge.

The relaxation time in reduced units is estimated as $\tau \sim 1$—that is, $\sim d^2/D$ in the original real-time (t) unit for $\lambda > d$. This means that the space-charge contribution would escape the detection limit or would give rise to a very low-frequency tail of the form $\varepsilon''(\omega) \sim 1/\omega$ when the cell thickness d became too large.

However, with decreasing cell thickness, as for a surface-stabilized ferroelectric liquid crystal (SSFLC) or even for a device application of a liquid-crystal cell where thin cells are required for lower operating voltages, the space-charge relaxation frequencies may enter the region of other low-frequency dielectric modes. Therefore it is important to study low-frequency dielectric effects of the ionic impurities to achieve a better understanding of overlapping low-frequency modes and to allow a detailed analysis of the device application characteristics.

2. Experimental procedure

Liquid-crystal 8CB was inserted into the gap between two flat glass plates coated with optically transparent and conductive indium tin oxide (ITO). The phase sequence of the liquid-crystal 8CB was confirmed to be as follows:

crystal–(21.1 °C)–smectic–(33.5 °C)–nematic–(40.8 °C)–isotropic.

For the samples, of both 4.5 μm and 1.6 μm cell thickness, homogeneous alignment was obtained by use of an alignment agent RN1155 with a subsequent rubbing of the alignment layer. Planar alignment was obtained for both samples, of 4.5 μm and 1.6 μm thickness, by use of either RN1155 (pretilt ∼1–2°) or SE3140 (pretilt ∼5–6°) alignment agent without rubbing of the alignment layer.

Temperature control was achieved with the sample on the heating stage (Linkam, LTS350) by use of an interfacing controller (Linkam, TMS 92) within the precision limit of ±0.1 °C, where the temperature scanning was run at the rate of 0.1 °C min^{-1}.

In situ observations of topological changes were made by use of a polarized-light optical microscope during the dielectric constant measurements as a function of temperature. Dielectric measurements were made by use of a standard capacitor and a digital lock-in amplifier system (EG&G, DSP7260) in the frequency range of 0.1 Hz to 200 kHz, where no intrinsic bulk mode has been found to appear in the 8CB liquid crystal [1,2]. In the 4.5 μm sample with planar alignment we observed a Schlieren texture in the nematic phase and a focal conic fan texture in the smectic phases. In the case of homogeneous alignments for both 4.5 μm and 1.6 μm samples we observed a uniform monochromatic form in the nematic phase but stripe patterns in the smectic phase with stripes parallel to the rubbing direction [7,8].

3. Experimental results and discussion

3.1. Dielectric constant

In figure 1 we have shown our data for the imaginary parts of dielectric constants obtained from two samples with different thicknesses of 4.5 μm and 1.6 μm, respectively. Peak frequencies of the dielectric loss are found at around 10 Hz and 100 Hz for the thick (4.5 μm) and thin (1.6 μm) samples, respectively. This thickness dependence of the peak frequency conforms with the space-charge relaxation time dependence on thickness. When this observed peak frequency was plotted as a function of temperature for both homogeneous and planar alignments of the 4.5 μm thick sample (figure 2(a)), we were able to see that the relaxation time was decreased

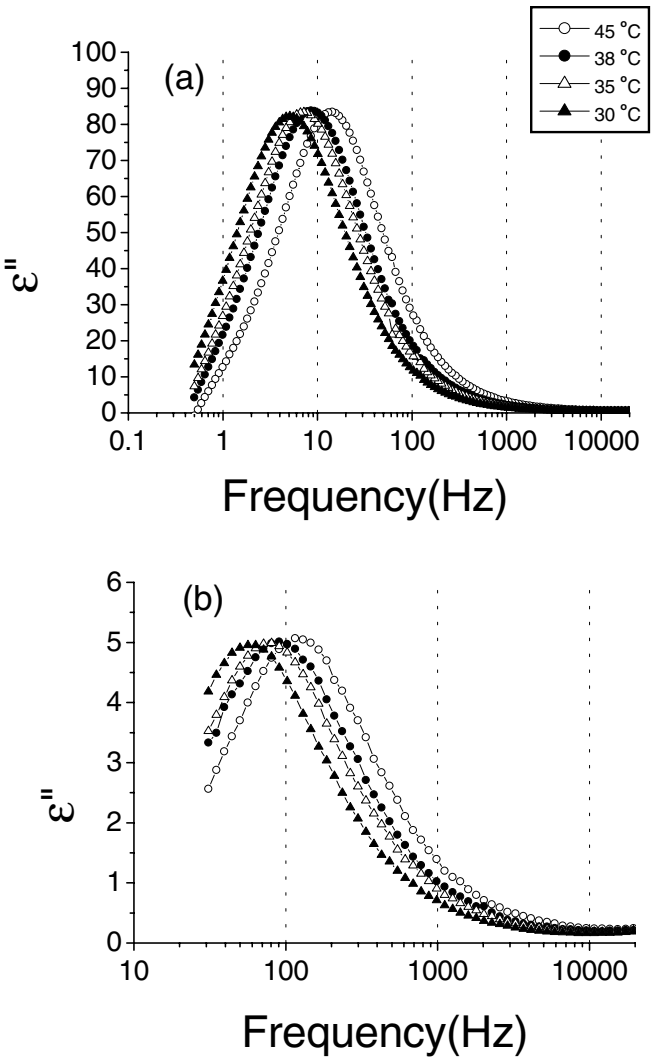

Figure 1. Dielectric loss constants ε'' observed as functions of frequency at selected temperatures for two different cell thicknesses: (a) 4.5 μm and (b) 1.6 μm.

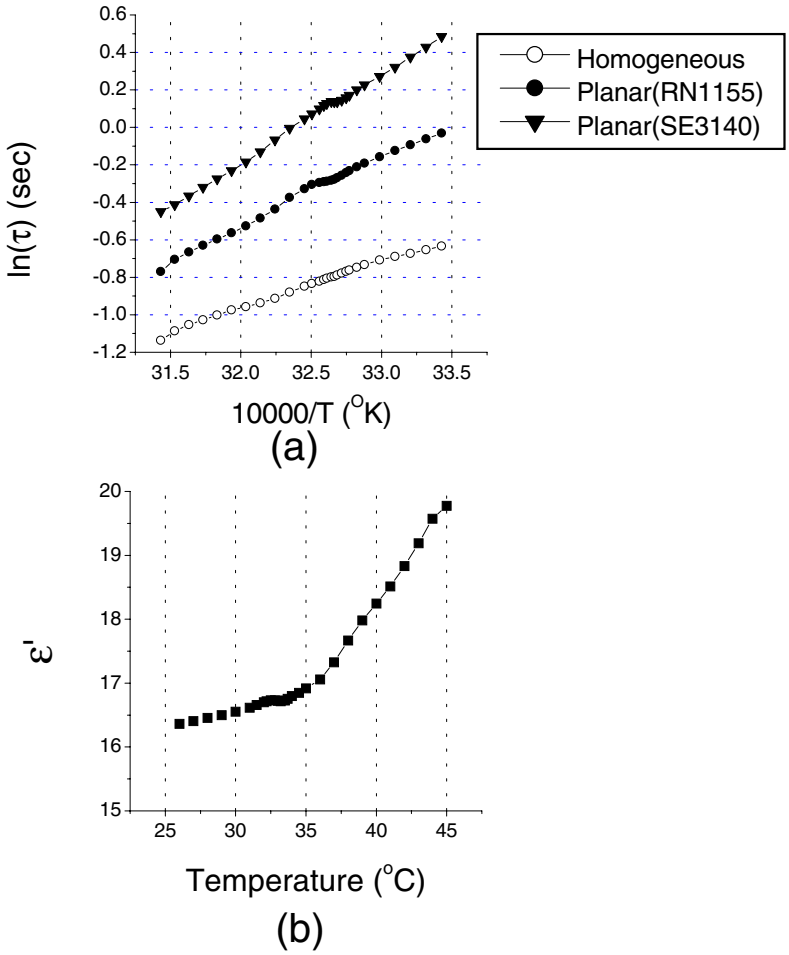

Figure 2. (a) Temperature dependences of dielectric relaxation times of 4.5 μm thick cells for both homogeneous and planar alignments and (b) the dependence of the dielectric constant (real part, ε') on temperature for the 4.5 μm sample with planar alignment (SE3140) measured at 6.4 kHz.

for the homogeneous alignment as compared with the planar alignment, in contrast to the expectation from the smaller diffusion constant for the homogeneous alignment. This implies an increased impurity concentration for the homogeneous alignment due to rubbing, since the conductivity relaxation time τ_c decreases with increasing impurity concentration n_0. Also from figure 2(a) we can see a general trend of increasing relaxation times with decreasing temperature, as expected from the Arrhenius behaviour of the diffusion constant dependence on temperature.

As can also be seen from figures 2(a) and 2(b), there is a dip in the curve across the nematic-to-smectic phase transition in the case of planar alignment, but a normal smooth change in the case of homogeneous alignment. This dip for the planar alignment may be ascribed to a phase transition enhancement of the diffusion constant. The effective diffusion constant for the planar alignment can be written as

$$D_{eff} = D_{\perp} + (D_{\parallel} - D_{\perp})\,\overline{\sin^2\theta}$$

and similarly for effective dielectric constant we have

$$\varepsilon_{eff} = \varepsilon_{\perp} + (\varepsilon_{\parallel} - \varepsilon_{\perp})\,\overline{\sin^2\theta}$$

where $\perp$ and $\parallel$ represent the vertical and the parallel direction respectively, with respect to the glass plane, θ the angle between the director of molecules and the glass surface. Since $\overline{\sin^2\theta}$ is expected to increase with the focal conic textural change of the nematic-to-smectic phase transition in the case of the planar alignment, we can expect both D_{eff} and ε_{eff} to increase with the transition to the smectic phase for the planar alignment. Figure 2(b) confirms this conjecture, where the dielectric constant of the liquid-crystal sample in the planar alignment with the SE3140 alignment layer is presented as measured at 6.4 kHz as a function of temperature.

Biradar *et al* [4] observed a low-frequency relaxation in their low-frequency dielectric measurements down to the sub-Hz region in a ferroelectric liquid crystal which they ascribed to charge accumulation in the surface alignment layer. This assignment was based on the observation by Hiller *et al* [9] that the low-frequency relaxation was not found in the case of magnetic field alignment without the surface alignment layer. However, their dielectric measurements were limited to above 100 Hz, and a dielectric relaxation due to ionic impurities should have been missed off at frequencies far below the lower limit of their measuring frequency range, since the relaxation time of ionic impurities increases in proportion to the square of the cell thickness. The present sample, 8CB, is a nonchiral liquid crystal, so we do not expect any low-frequency bulk mode and we have the homeotropic alignment even without the surface alignment layer. For this homeotropic alignment without the alignment layer, we observed a low-frequency dielectric relaxation in the 8CB sample, which was found to depend on the sample thickness and thus a diffusion process of ionic impurities.

In figures 3 and 4 we have shown normalized dielectric dispersion data observed for both 4.5 μm and 1.6 μm samples at a fixed temperature of 30 °C. With the 1.6 μm sample (figure 4) we can hardly see any change with changing external-field strength but we can see for the 4.5 μm sample (figure 3) that the relaxation peak shifts toward lower frequencies with increasing external-field strength. This observation suggests that the ionic impurity relaxation goes beyond a simple diffusion since the peak frequency is expected to shift toward higher frequencies with increasing field strength in the field-assisted diffusion. In the following section we want to show that this problem may be solved with the addition of a competing ionization–recombination term.

3.2. Diffusion of impurities under ionization–recombination reactions

For real liquid-crystal cells, ionic impurity concentrations are determined by reactions between ionization and recombination competing [10] to maintain a thermodynamic equilibrium as follows:

$$\mathrm{AB} \rightleftharpoons \mathrm{A}^+ + \mathrm{B}^-$$

so equation (1) may be modified to include the reaction terms:

$$\frac{\partial n}{\partial t} = \beta N_0 - \alpha np + D_n \frac{\partial^2 n}{\partial x^2} - \mu_n \frac{\partial}{\partial x}\left(n \frac{\partial V}{\partial x}\right) \tag{3}$$

and similarly for p:

$$\frac{\partial p}{\partial t} = \beta N_0 - \alpha np + D_p \frac{\partial^2 p}{\partial x^2} + \mu_p \frac{\partial}{\partial x}\left(p \frac{\partial V}{\partial x}\right) \tag{4}$$

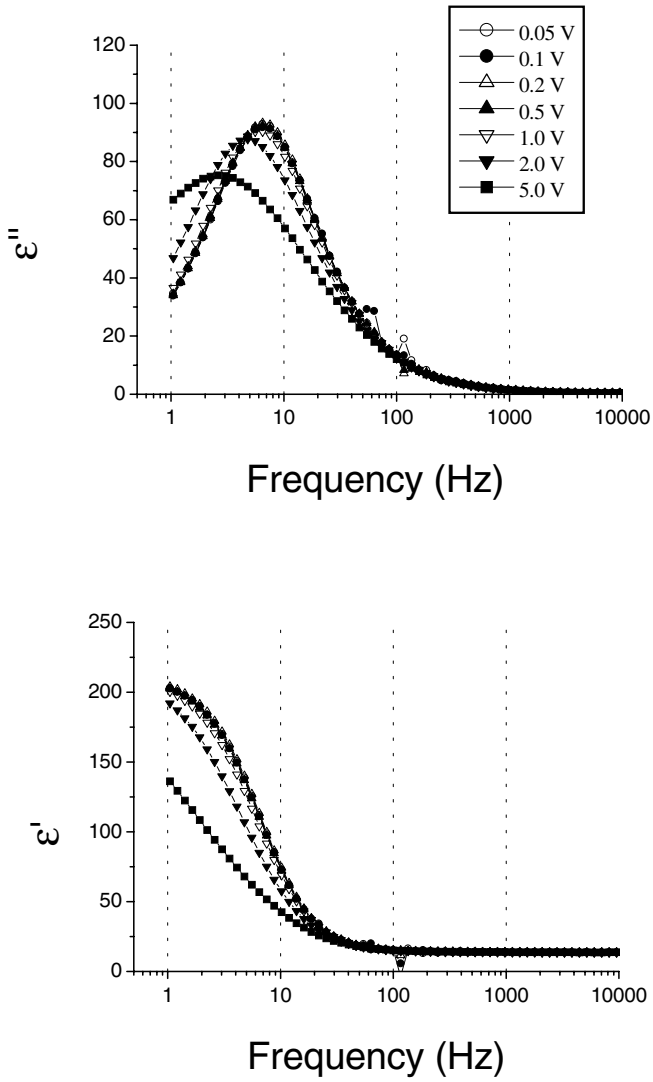

Figure 3. Dielectric constant dependence on frequency for the 4.5 μm cell with homogeneous alignment measured at various field amplitudes of sinusoidal external fields: (a) the imaginary part (ε'') and (b) the real part (ε'), where data values are normalized to the unit field strength for various applied-field amplitudes.

where n and p represent negative- and positive-charge ionic concentrations, $\beta(E)$ the ionization rate, α the recombination rate, N_0 the impurity density, and V the electric potential. The equilibrium charge densities for zero external field ($E = 0$) are given by

$$n_0 = p_0 = \sqrt{\frac{\beta(E=0)N_0}{\alpha}}. \tag{5}$$

Ionization in the system is a thermal activation process and can be written as

$$\beta(E) = \beta_0 \exp(-(U_0 - \Delta U)/k_B T)$$

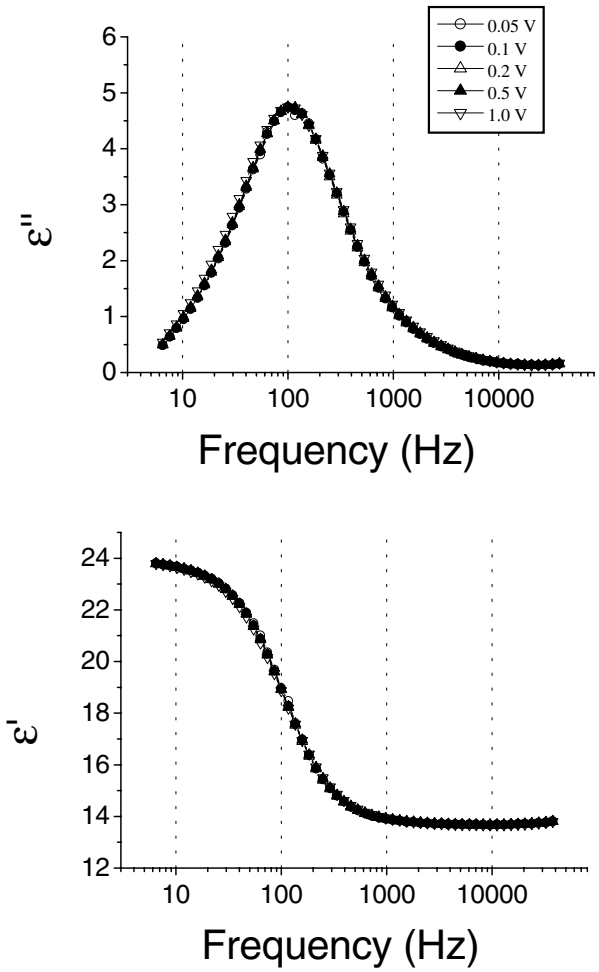

Figure 4. Dielectric constant dependence on frequency for the 1.6 μm cell measured at various field amplitudes of sinusoidal probe fields: (a) the imaginary part (ε'') and (b) the real part (ε').

where U_0 represents the activation energy barrier, $\Delta U(E) = q\sqrt{qE/\pi\varepsilon}$ a change in the activation barrier caused by an external field E, and q the ionic charge. With the following changes of variables:

$$x/d \to x \qquad t/\tau_0 \to t \qquad n/n_0 \to n$$
$$p/p_0 \to p \qquad V/V_0 \to V$$

where d is the sample thickness, $\tau_0 = d^2/D_n$, and $V_0 = en_0d^2/\varepsilon$, we can obtain the following equations in reduced variables in dimensionless units:

$$\frac{\partial n}{\partial t} = \kappa(\exp(\gamma\sqrt{V}) - np) + \frac{\partial^2 n}{\partial x^2} - \delta^2 \frac{\partial}{\partial x}\left(n\frac{\partial V}{\partial x}\right) \tag{6}$$

$$\frac{\partial p}{\partial t} = \kappa(\exp(\gamma\sqrt{V}) - np) + \eta\frac{\partial^2 p}{\partial x^2} + \eta\delta^2 \frac{\partial}{\partial x}\left(p\frac{\partial V}{\partial x}\right) \tag{7}$$

$$\frac{\partial^2 V}{\partial x^2} = (n - p) \tag{8}$$

where

$$\kappa = \alpha n_0 d^2 / D_n$$
$$\eta = D_p / D_n$$
$$\delta^2 = e n_0 \mu_n d^2 / D_n \varepsilon$$
$$\gamma = (q/k_B T) V_0 / d\sqrt{q/\pi\varepsilon}.$$

For the small-field regime we write $n = 1 + \nu_n$, $p = 1 + \nu_p$, and assume slow ions (p) to have a vanishing mobility ($\mu_p = 0$). Furthermore, in the simplest case of $\kappa \ll 1$—that is, where the ionization–recombination process is much slower than the diffusion process of fast ions (n)—we may neglect direct-coupling terms to obtain decoupled equations for $p(t)$ and $n(t)$. Since p (slow ions) is assumed to change very slowly, we can put $p \simeq 1$ to obtain in the small-field approximation

$$\frac{\partial \nu_n}{\partial t} = -\kappa \nu_n + \frac{\partial^2 \nu_n}{\partial x^2} - \delta^2 \nu_n. \tag{9}$$

This equation is equivalent to the case of no ionization–recombination process with a simple substitution of $\delta^2 + \kappa$ for δ^2. From the data of Chieu and Yang [10], where $d = 1.6 \times 10^{-4}$ cm, $n_0 = 10^{15}$ cm^{-3}, $D_n = 6.63 \times 10^{-6}$ cm^{-2} s^{-1}, $\mu_n = 8.5 \times 10^{-7}$ cm^2 V^{-1} s^{-1}, and $\varepsilon = 5\varepsilon_0$, we can estimate $\delta^2 \simeq 1$. This means that for fast ions (n) with $\kappa \ll 1$ the ionization–recombination process hardly affects the dielectric constant (see equation (2)) except that there is a very small change of the δ^2-value to $\delta^2 + \kappa$.

However, for slow ions (p) our approximations lead to

$$\frac{\partial \nu_p}{\partial t} = -\kappa(\nu_p + \nu_n). \tag{10}$$

If we neglect the ν_n-dependence on time in this low-frequency long-time limit, the relaxation time of slow ions (ν_p) can be found as $\tau_p \simeq 1/\kappa$. This relaxation time will then decrease as κ increases. The corresponding relaxation peak will then shift to higher frequency and eventually overlap with the relaxation peak of fast ions at a certain value of κ above a crossover threshold. When we meet this situation, however, we can no longer assume the decoupling between ν_n and ν_p. The coupled equations should be solved in this case by a numerical method.

3.3. Numerical simulation

We can solve the coupled equations (equations (6), (7), and (8)) for more general values of parameters by a numerical calculation. Numerical simulation for the response function of the system coupled to an external field was carried out as follows. The system was partitioned into 20 cells ($\Delta x = 0.05$) with initial densities all set to 1. The density change in each cell on turning on the external field was followed as a function of time by considering the local ionization–recombination process, diffusions from neighbour cells, and field-induced drift motions. The Poisson equation was solved by use of the successive over-relaxation method [11], and the frequency dependence of the ionic polarization response was calculated from

$$\varepsilon(\omega) = \frac{1}{VT} \int \int_0^T x(p - n) \mathrm{e}^{\mathrm{i}\omega t} \, \mathrm{d}t \, \mathrm{d}x$$

where $n(t)$ and $p(t)$ were averaged over one period T of the external electric field after sampling over periods, V is the voltage amplitude, and x is the coordinate in the direction of the sample thickness.

In figure 5 we have shown responses to external fields of varying field strength and frequency for the system with $\mu_p = 0$, $\gamma = 0.1$, and various combinations of δ and κ. Although we have $\gamma \propto n_0 d \propto \sqrt{d}$, the γ-dependent terms $\exp(\gamma\sqrt{V})$ are reduced to ~ 1 in the small-field regime $V \ll 1$ of dielectric constant measurements. The numerical results were found to be almost the same between $\gamma = 0.1$ and $\gamma = 0.2$. The three parameters γ, δ, and κ are all dependent on d, but κ/δ^2 can be seen to be independent of d. However, κ proportional to α is more like a measure of the recombination process and δ^2 is purely a cell parameter representing for impurity density as well as thickness of the cell. Since we have $\delta^2 \simeq 1$ for $d = 1.6$ μm [10] we can take $\delta^2 \simeq 10$ for $d = 4.5$ μm. If we set $\kappa = 10$ for the 1.6 μm sample we may take a larger value of $\kappa = 100$ for the 4.5 μm sample since $\kappa \propto n_0 d^2$.

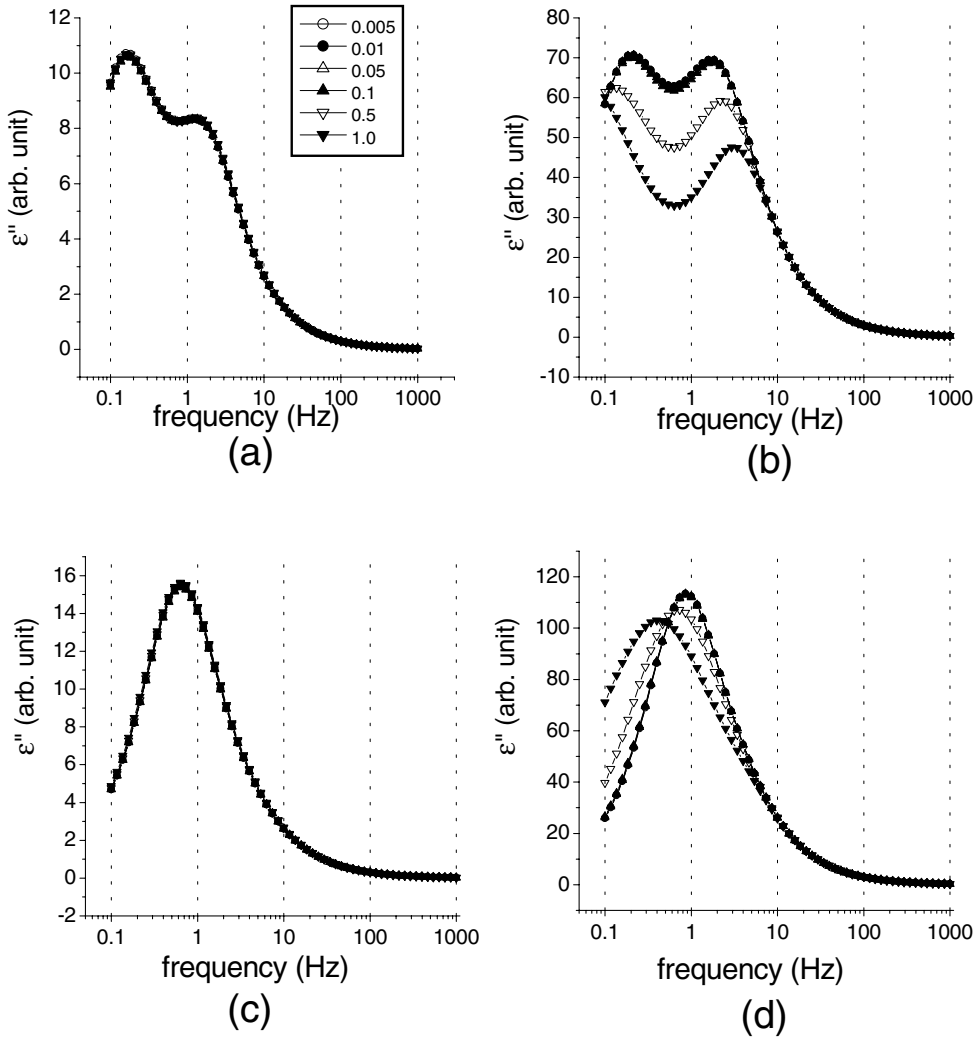

Figure 5. Imaginary-part dielectric constant data dependence on frequency obtained from numerical simulations including ionization–recombination terms at various field amplitudes of the sinusoidal probe field for selected parameter values of (a) $\kappa = 1$, $\delta^2 = 1$, (b) $\kappa = 1$, $\delta^2 = 10$, (c) $\kappa = 10$, $\delta^2 = 1$, (d) $\kappa = 100$, $\delta^2 = 10$.

As can be seen from figures 5(a) and 5(b), we have two relaxation peaks for $\kappa/\delta^2 \leqslant 1$, one at 0.1 Hz corresponding to slow ions (p) and another at 2 Hz corresponding to fast ions (n). However, with $\kappa/\delta^2 = 10$ the two peaks overlap as can be seen from figures 5(c) and 5(d) due to increased relaxation frequency of slow ions (p). In the case of $\kappa = 1$ and $\delta^2 = 10$ (see figure 5(b)), we can see that the slow ions show a relaxation peak at lower frequencies with increasing field strength due to the ionization–recombination process, whereas the fast ions tend to show a relaxation peak at higher frequencies with increasing field strength. On the other hand, with $\kappa = 1$ and $\delta^2 = 1$ (see figure 5(a)) no field-dependent dispersion was introduced by the same changes of field strength. For $\kappa = 10$ we have more confirmative results of no field dependence with $\delta^2 = 1$ (see figure 5(c)).

Referring to figure 3, where dielectric responses of homogeneously aligned samples at 30 °C are shown for both thick (4.5 μm) and thin (1.6 μm) samples at various external fields, we can observe no field-dependent dispersion with a thin sample of small δ-value, but the thick sample with a large δ-value shows a field dependence of the peak frequency. The experimental results of figure 3 conform with the numerical calculations with $\kappa = 100$ and $\delta^2 = 10$, while the results of figure 4 conform with the case of $\kappa = 10$ and $\delta^2 = 1$. This field-dependent dispersion in thick samples, however, cannot be explained by a simple diffusion process without ionization–recombination reaction, where we expect an opposite direction of frequency shifts.

When we define a characteristic time for the ionization–recombination process τ_K, a peak frequency of the slow ionic dielectric response ω_p, and another response peak frequency of the fast ions ω_n, we can differentiate three different regimes of dielectric response. In the case of $\tau_K^{-1} < \omega_p < \omega_n$ we expect two separate peaks, both of which will be shifted to higher frequencies with increasing field strength. In the case of $\omega_p < \tau_K^{-1} < \omega_n$ we still have two peaks; the lower-frequency peak due to the ionization–recombination process of the slow ions will shift further to the lower-frequency side while the higher-frequency peak of the fast ions will shift further to the high-frequency side with increasing field strength. In the case of $\omega_p < \omega_n < \tau_K^{-1}$ we expect to observe one single peak, shifting to the low-frequency side with increasing field strength due to the ionization–recombination effect.

We can understand this field-dependent behaviour of low-frequency relaxation peaks when ionization–recombination is a dominant process from the following pictures. When the field is applied, positive and negative ions will tend to drift toward negative and positive electrodes respectively. The negative and positive ions are thus separated further, and the recombination process will be accordingly reduced. The field due to the polarization will decrease the effective field and thus reduce the ionization process. In the slow regime of the low-frequency limit we can thus expect separated fast ions to move faster with increasing field while slow ions moving through the ionization–recombination steps will become slower due to the effective reduction of the ionization–recombination rate with increasing field strength. This separation of fast and slow ions corresponds to the emergence of two peak structures in the dielectric response.

We have also made a best fit to the experimental data for the thick (4.5 μm) sample of

$$\varepsilon(\omega) = \frac{\Delta\varepsilon}{1 + (\mathrm{i}\omega\tau)^{1-\alpha}} + \varepsilon_\infty \tag{11}$$

to find the field strength dependence of the peak frequency $\omega_m = 2\pi/\tau$ and the width parameter α. In figure 6 we have shown the best-fit results for the peak frequency ω_m and width parameter α obtained from equation (11) best fitted to experimental data (figures 3(a) and 3(b)) and numerical data (figures 5(c) and 5(d)) as functions of applied-field amplitude. A drastic decrease of peak frequency and a sudden increase of peak width at a threshold field are precursors to a crossover to two separated peak structures.

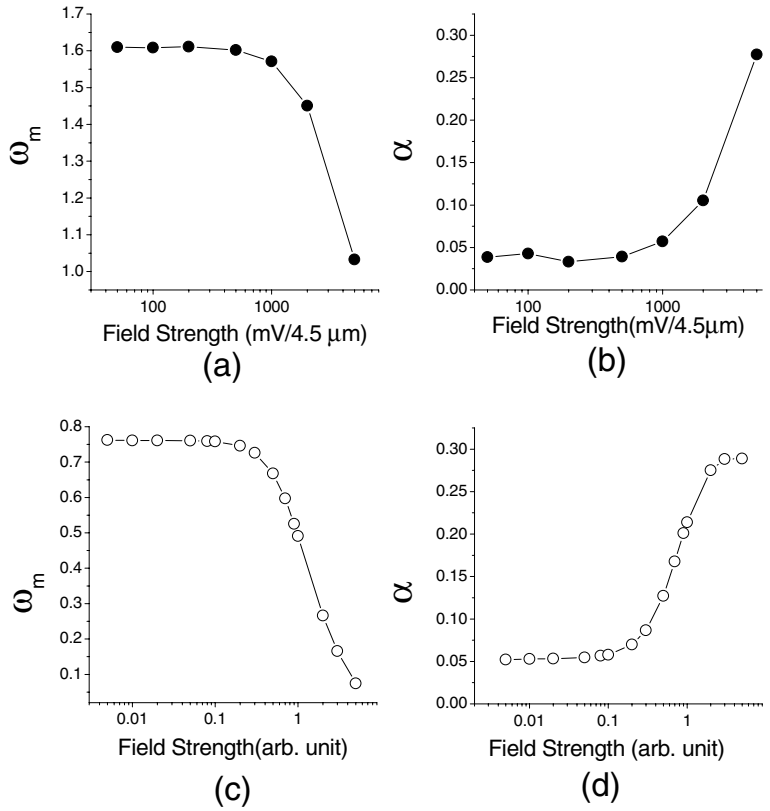

Figure 6. Field strength dependence of the peak frequency (ω_m) and bandwidth parameter (α) obtained from the best fits of (a)/(b) experimental data and (c)/(d) numerical simulation data (with $\kappa = 100$, $\delta^2 = 10$) to equation (11) for the 4.5 μm thick cell.

4. Conclusions

We have measured dielectric constants of a liquid crystal, 8CB, for two different cells of thickness 4.5 μm and 1.6 μm. When the external field was increased in the 4.5 μm sample, we observed an anomalous shift of peak frequencies to the low-frequency side. The external-field dependence of the dielectric response was also studied by use of a numerical simulation considering an ionization–recombination term. The results of numerical simulations predicted a low-frequency relaxation peak shifting toward the low-frequency side with increasing field strength instead of the high-frequency side as predicted for a simple diffusion process. This low-frequency relaxation, attributed to the ionization–recombination-assisted diffusion in the limit of zero mobility of slow ions, could explain our experimental observation for 8CB. This space-charge relaxation can thus show a different dielectric spectrum—from a single peak to two separated peaks—depending on the relative dominance of the diffusion and the ionization–recombination terms.

Acknowledgment

This work was supported in part by the Korea Research Foundation, Grant (KRF-2000).

References

[1] Druon C and Wacrenier J M 1983 *Mol. Cryst. Liq. Cryst.* **98** 201
[2] Warcrenier J M, Druon C and Lippens D 1981 *Mol. Phys.* **43** 97
[3] Ashcroft N W and Mermin N D 1976 *Solid State Physics* (New York: Holt, Rinehart and Winston) p 16
[4] Biradar A M, Kilian D, Wrobel S and Haase W 2000 *Liq. Cryst.* **27** 225
[5] Sinha G P and Aliev F M 1998 *Phys. Rev.* E **58** 2001
[6] Coelho R 1979 *Physics of Dielectrics for the Engineer (Fundamental Studies in Engineering vol 1)* (Amsterdam: Elsevier Scientific) p 97
[7] Crawford G P, Geer R E, Naciri J, Shashidhar R and Ratna B R 1994 *Appl. Phys. Lett.* **65** 2937
[8] Sprunt S, Selinger J V, Crawford G P, Ratna B R and Shashidhar R 1995 *Phys. Rev. Lett.* **74** 4671
[9] Hiller S, Biradar A M, Wrobel S and Haase W 1996 *Phys. Rev.* E **53** 641
[10] Chieu T C and Yang K H 1989 *Japan. J. Appl. Phys.* **28** 2240
[11] Smith G D 1985 *Numerical Solution of Partial Differential Equations* 3rd edn (Oxford: Oxford University Press)